Proc. of SPIE Vol. 3355, Optical Astronomical Instrumentation, ed. S D'Odorico (Jun 1998) Copyright SPIE

Elastomeric Lens Mounts

T. S. Mast, P. I. Choi, D. Cowley, S. M. Faber, E. James, and A. Shambrook

University of California / Lick Observatories
University of California, Santa Cruz, CA 95064

ABSTRACT

Instruments for large telescopes often require cameras with large, deeply-curved, and temperature-sensitive lenses. The instrument error budgets require each lens to be supported so that excellent performance is maintained in the face of gravitational and thermal perturbations. We describe here elastomeric mounts that address these requirements. We first describe the general design principles, the effects of errors in design and fabrication, and the performance under static and dynamic loads. We describe specific examples; the elastomer RTV560 and the lens supports for the camera of the W. M. Keck Observatory DEIMOS spectrograph.

Keywords: lens, mount, elastomer, RTV560, DEIMOS, camera

1. INTRODUCTION

As telescopes have increased in size, so have many of their instruments. Cameras for these instruments include large, deeply-curved, and temperature-sensitive lenses. The instrument error budgets require each lens to be supported so that excellent performance is maintained in the face of gravitational and thermal perturbations. We describe here elastomeric mounts that address these requirements. Sections 2 and 3 discuss general design principles and the effects of errors in the mount design. The performance of these mounts under static and dynamic loads is discussed in Section 4. We then describe specific examples; the elastomer lens supports for the camera of the W. M. Keck Observatory DEIMOS spectrograph. We have selected the elastomer RTV560, a product of GE Silicones (Waterford, NY).

Many designs have been used to support lenses and groups of lenses. Yoder (1993, 1997) gives an overview of a variety of designs in use. The specific requirements and specific lens geometry determine each particular design. This is also true for the elastomeric designs described here. Thus the general design principles given below can only cover a limited range of applications.

Elastomer mounts can serve several functions at the same time. They can provide:

1. positioning support against gravity loads; fixed and changing, axial and radial
2. a low stress response to temperature changes
3. a dam to contain optical coupling fluids

2. DESIGN PRINCIPLES

Consider a single circular lens supported around its circumference within a circular mount. The thermal expansion coefficients of the lens and mount typically differ, and temperature changes can induce radial

forces on the lens. Depending on the lens size and shape and the lens and mount material properties, these forces might deform or even break the lens.

One response to this is to use an elastomer buffer between the lens and the mount. This elastomer serves to bond the lens in the mount and maintain a stress-free spacing between the lens and mount as the temperature changes.

The radial thickness of the elastomer (difference between the lens and mount radii) can be chosen so that its expansion with temperature matches the expansion of the gap between the lens and mount. With this radial thickness no radial forces are imposed as the temperature changes.

The axial width of the elastomer can be chosen to tailor the motion of the lens under gravity loads. In this report we assume the elastomer is azimuthally continuous. Additional tailoring to thermal and gravity loads is possible by varying the width with azimuth.

In the following we refer to the lens and mount as "glass" and "metal;" the actual materials may vary.
Define $T_o \equiv$ the fabrication temperature,
$\Delta T \equiv T - T_o \equiv$ deviation from the fabrication temperature,
$R_{om}, R_{og} \equiv$ periphery radii of the metal and glass at fabrication temperature,
$\alpha_m, \alpha_g, \alpha_e \equiv$ linear thermal expansion coefficients for metal, glass, elastomer.

The glass-to-metal distance $\equiv t_{g\text{-}m}(T) = (R_{om} - R_{og}) + (R_{om}\alpha_m - R_{og}\alpha_g)\Delta T.$ (1)

The elastomer thickness $\equiv t_e(T) = (R_{om} - R_{og}) + (R_{om} - R_{og})\alpha_e \Delta T.$ (2)

To have a stress-free design these two distances must match $\Rightarrow t_e(T) = t_{g\text{-}m}(T)$,

$$(R_{om}\alpha_m - R_{og}\alpha_g) = (R_{om} - R_{og})\alpha_e .$$

Define $t_{oe} \equiv (R_{om} - R_{og}) =$ the elastomer thickness at T_o.

$$t_{oe} = \frac{R_{og}(\alpha_m - \alpha_g)}{(\alpha_e - \alpha_m)} \quad \text{or} \quad t_{oe} = \frac{R_{om}(\alpha_m - \alpha_g)}{(\alpha_e - \alpha_g)} . \tag{3}$$

The above equations assume the following:

1. At T_o the elastomer exactly fills the gap between glass and metal.
   (The casting at T_o leaves the elastomer free of stress.)
2. Strains are linearly proportional to ΔT for the glass, metal, and elastomer.
3. The α's are constants, independent of T and t_{oe}.

In practice, this simple description needs to be modified because the elastomer thermal expansion coefficient is itself a function of the thickness, $\alpha_e(t_{oe})$. As described below in Section 5, for the geometries of interest here we can accurately write

$\alpha_e(t_{oe}) = \beta + \gamma t_{oe}$, where β and γ are constants defined in Section 5. (4)

Solution of Equation 3 for t_{oe} gives

$$t_{oe} = \frac{1}{2\gamma}\left[-(\beta - \alpha_m) + \left[(\beta - \alpha_m)^2 + 4\gamma R_{og}(\alpha_m - \alpha_g) \right]^{1/2} \right] . \tag{5}$$

3. DESIGN AND FABRICATION ERRORS

An athermalized design is made using design values of the α's and R's in Equation 5. However, if the physical values of the α's or R's are different, then the glass-to-metal gap will not match the elastomer gap for non-zero ΔT. We define errors for each quantity. For example

$$R_{og}^{phys} \equiv R_{og}^{des} + \delta R_{og} .$$

An error in measuring the glass would create a non zero δR_{og}. An error in the knowledge of α_m would create a non zero $\delta\alpha_m$.

Define the mismatch between the glass-metal gap and the RTV thickness to be

$$M \equiv t_e(T)^{phys} - t_{g\text{-}m}(T)^{phys} . \tag{6}$$

For each error Equations 1, 2, and 6 give the following:

$$\begin{aligned}
&\delta R_{om}: && M = \delta R_{om} (\alpha_m - \alpha_e) \Delta T \\
&\delta R_{og}: && M = -\delta R_{og} (\alpha_g - \alpha_e) \Delta T \\
&\delta \alpha_m: && M = \delta \alpha_m R_{om} \Delta T \\
&\delta \alpha_g: && M = -\delta \alpha_g R_{og} \Delta T \\
&\delta \alpha_e: && M = -\delta \alpha_e (R_{om} - R_{og}) \Delta T
\end{aligned} \tag{7}$$

where $\delta\alpha_e$ arises from $\delta\beta$, $\delta\gamma$, or both

These M's induce stress in the glass, metal, and elastomer where the magnitudes depend on the elastic moduli. Since E_m = ~10 x 10^6 psi, E_g= ~10 x 10^6 psi, and E_e = ~300 to ~10^4 psi, we can assume that the stress deforms primarily the elastomer. This stress is given by

$$\sigma = E_e \frac{M}{t_{oe}} . \tag{8}$$

The following is a procedure for calculating the impact of the errors:

1. Determine E_e and σ using Equations 7 to 8.
2. Using the stress σ as input, make a finite-element calculation of the deformations induced on the particular lens.
3. Fit the node motions from the finite-element calculation to smooth functions (for example, Zernike polynomials).
4. Use these surface aberrations as input to a ray-trace analysis to calculate the optical consequences.

4. ELASTOMER PROPERTIES

Elastomers are nearly incompressible and this strongly controls their behavior. If some surfaces are constrained (for example bonded to metal or glass), the effective E and α depend on the detailed geometry of the constraints. Gent and Lindley (1959) derived an expression for E for constrained geometries and tested it with measurements. The constrained elastic modulus is the unconstrained modulus times a factor that depends on the constraint geometry. $E = E_0 F(S)$, where S is the ratio of the area of one constrained

face to the total force-free area. The ratio is traditionally called the "shape factor." For an infinitely long elastomer bead of width w and thickness t, Gent and Lindley derive

$$E_c = 4 E_0 (1 + S^2) / 3 \qquad \text{where } S = w/(2t).$$

Later Lindley (1972) fit empirical data by adding a "material factor" (k) to the expression.

$$E_c = 4 E_0 (1 + kS^2) / 3$$

Lindley gives values of k that depends on the hardness, E, G, or K. For example, for a Shore A durometer = 55, elastic modulus = 460 psi, amd shear modulus = 115 psi , k = 0.64.

The shear stress is given by the usual relation, $g = G \phi$, and since Poisson's ratio for an elastomer is close to 0.5, to a good approximation $G = E_c/3$. The bulk compressive stress is defined by the usual expression, $p = -K \frac{dV}{V}$, and for elastomers K is typically >> E.

The fractional change in thickness with a temperature change ΔT, is given by $\frac{\delta t}{t} = \alpha \Delta T$. For elastomers the effective α also depends strongly on the geometry of the bond constraints, in particular the shape factor, S. We have found no theoretical derivation of this dependence. Lobdell (1968) describes α by a function $\alpha = \alpha_o K_T (S)$, where $K_T(0) = 1$. Given the empirical nature of these relationships, we concluded that we needed to measure the properties of the elastomer for the bond geometry of each lens.

5. AN EXAMPLE: THE ELASTOMER RTV560

For mounting the lenses of the DEIMOS spectrograph we have followed Fata and Fabricant (1993) and chosen RTV560 by GE Silicones. This elastomer has a high strength (4.8×10^6 N m^{-2} in tension), tolerates a wide temperature range (-115 ^oC to 260 ^oC), has low shrinkage (1.0 %), and has a viscosity suitable for precision machining.

We prepared samples (Table 1) using RTV560 and measured the elastic modulus and thermal expansion coefficient. The "shape factor" is defined

$$S = \frac{w}{2t} \quad \text{where w is the width and t the thickness of the RTV bond.} \qquad (9)$$

We assumed the length is long to match the thin circular bead around the DEIMOS lenses. The values of S varied from 0.48 to 7.33. The RTV560 was cast between a plate of brass and a plate of aluminum, each 0.25 inches thick. A dam was used in the casting and was removed after the RTV560 cured.

To measure the thermal coefficient we cooled the samples an average of 14 ^oC from room temperature using ice water, and we measured the contraction using a Mitutoyo linear gauge (resolution = 1 micron). The resulting α's are shown in Table 1 and Figure 1. The errors are estimated using thickness measurement errors of 1 micron and temperature errors of 0.5 ^oC at both temperatures of the measurement.

We measured the elastic modulus using the same samples. Each sample was loaded with a succession of 25 pound weights. A compliance of the setup was measured and subtracted from the measured displacements. In addition, the first two weights induced a measured displacement by bending the metal

plates. Additional loads of 25 pounds each resulted in a linear relationship between stress and strain. The slope of this linear relationship is reported in Table 1. Uncertainties in the sample-support elasticity and the measurement errors prohibited measurements for the two samples with the highest S values. The errors for E reported in Table 1 are statistical only, based on the displacement measurement error. Systematic errors probably dominate the true error.

Table 1. RTV560: Measured Elastic Modulus and Thermal Expansion Coefficient

Sample	t (inch)	w (inch)	l (inch)	S	E_e (psi)	$\alpha_e \times 10^{+6}$ (/deg C)
1	0.063	0.25	12.0	1.94	1900 ± 260	690 ± 53
2	0.063	0.50	12.0	3.81	-	749 ± 68
3	0.063	1.00	12.0	7.33	-	817 ± 60
4	0.177	0.25	12.0	0.69	664 ± 12	497 ± 26
5	0.177	0.50	12.0	1.36	1287 ± 88	616 ± 32
6	0.177	1.00	12.0	2.61	2291 ± 557	659 ± 35
7	0.253	0.25	12.0	0.48	603 ± 7	412 ± 22
8	0.253	0.50	12.0	0.95	776 ± 22	544 ± 26
9	0.253	1.00	12.0	1.82	1267 ±557	598 ± 27

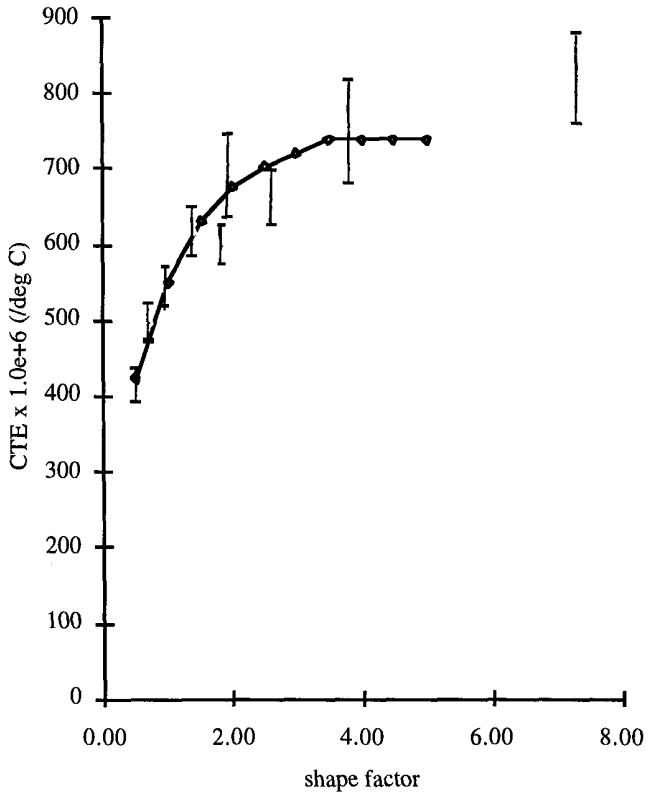

Figure 1. Measured Thermal Coefficient for RTV560 as a function of shape factor. The points with errors are our measurements of RTV560. The open points connected by lines are the measurements by Lobdell (1968) for RTV11, shown for comparison.

A chisqure fit of these data to $\alpha(S) = A + B/S$ yields

$$A = (723 \pm 10) \times 10^{-6}\ /^{o}C \text{ and } B = (-168 \pm 8) \times 10^{-6}\ /^{o}C. \quad (10)$$

In terms of the notation of Equation 4 and using S = w/2t

$$\alpha_e(t_{oe}) = \beta + \gamma t, \qquad \beta = A, \qquad \gamma = \frac{2B}{w}. \quad (11)$$

The incompressibility of the material implies $\alpha(S = \infty) = 3 \times \alpha(S=0)$. G. E. Silicones gives $\alpha(S=0) = 200 \times 10^{-6}\ /^{o}C$. Our measurement of A (723 ± 10) is 20% higher than expected. The source of this difference is unknown. Possible sources include a systematic error in the measurements and variations in the elastomer materials properties with temperature, humidity, curing environment, and curing time.

Lobdell (1968) measured the thermal expansion coefficient of RTV11 for values of S varying from 0.48 to 4.51 (Figure 1). The values of the thermal expansion coefficient fit

$$\alpha_e(S) = 768 - 184 / S \qquad [\ (10^{-6}/\ ^{o}C)\ ] \qquad \text{with an rms residual of 3\%.} \quad (12)$$

Equation 10 is valid for S > 0.5, the range of the measurements. The lens elastomer designs in Section 6 and those of Fata and Fabricant (1993) call for S values within this range. Equation 10 is not valid for values of S less than 0.5, corresponding to nearly unconstrained geometries (S ~ 0), where α_e is approximately the value cited by the manufacturer.

Our measurements of the elastic modulus were fit to $E = 4E_o(1+kS^2)/3$ and yielded

$$k = 0.38 \text{ and } E_o = 497 \text{ psi with an rms of 15 \%.} \quad (13)$$

6. AN EXAMPLE: THE DEIMOS SPECTROGRAPH FOR W. M. KECK OBSERVATORY

The DEIMOS spectrograph is being designed and built by UCO/Lick Observatories at the University of California, Santa Cruz. It will measure simultaneous spectra of up to about 100 objects. The camera optics in the spectrograph were designed by Epps (1995). The design calls for five lens groups with nine lenses (Figure 2).

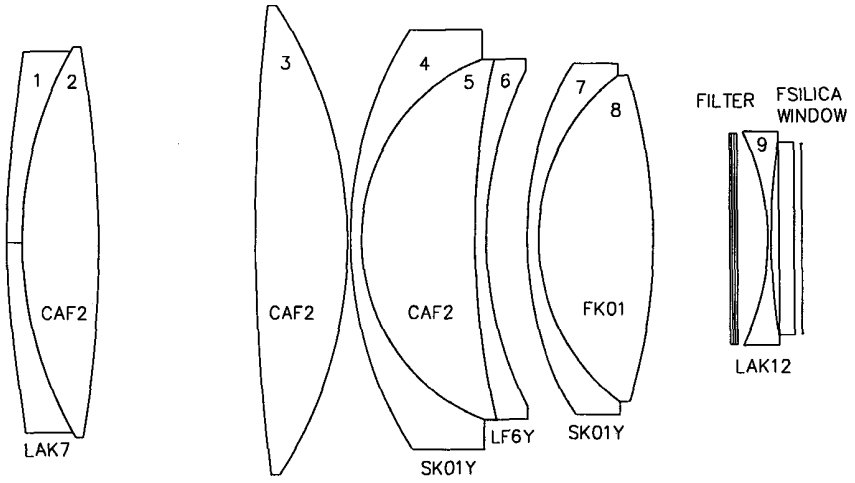

Figure 2. Layout of the DEIMOS camera lenses.

Descriptions of preliminary designs for these mounts are given by Faber et al. (1996). In the final design we will optically couple the lenses within each group using a fluid couplant. We have chosen to mount the glass lenses (1,4,6,7,8) in stainless steel (SS303) to match the camera barrel. Lens 9 is mounted on the aluminum vacuum vessel for the detector and will be mounted in an aluminum ring.

The glass lenses will be mounted using RTV 560. For those in groups, the RTV560 will also serve to constrain the optical fluid. Elements 2, 3, and 5 are CaF_2. For these, the α is so high that it nearly matches the SS303. Thus the elastomer gap stays fixed, and the elastomer goes into tension at low temperature, inducing an expansive stress in the fragile CaF_2, which is undesirable. Since Element 3 is a singlet, for which no fluid couplant needs to be contained, we can simply use Delrin pads between the lens and mount. Element 5 is the central element of a triplet and is supported by the two outer elements; no elastomer support is needed. For the remaining CaF_2 Element 2 we have designed a special mount (using preloaded RTV) that is not athermalized, but maintains a compressive load on the CaF_2 down to the lowest expected temperature ($-15^{o}C$). The expected stress due to preloading is small (about 30 psi).

Table 2a gives the material, R_{og}, α_g, and E_g for each lens to be mounted in an athermalized elastomeric mount. Table 2b gives the RTV560 dimensions w and t, the shape factor S, and α and E for the RTV560. The values of t and R_{om} are based on Equations 5, 10, and 11. We have used values for the width w that a approximately the available free edge of the lens.

Table 2a. DEIMOS Camera: Glass and Metal: R, α, and E for each lens.

Lens	Schott Name	Ohara Name	R_{og} (inches)	α_g x 10^6 (/ ^{o}C)	E_g x 10^{-6} (psi)	α_m x 10^6 (/ ^{o}C)	E_m x 10^{-6} (psi)	cell material
1	LaK7	LAL7	6.10	6.7	13.9	18.7	28.0	SS303
4	SK01Y	BSM51Y	6.70	6.3	13.1	18.7	28.0	SS303
6	LF6W	PBL26Y	5.75	8.9	8.5	18.7	28.0	SS303
7	SK01Y	BSM51Y	5.60	6.3	13.1	18.7	28.0	SS303
8	FK01	FPL51	5.20	12.7	10.8	18.7	28.0	SS303
9	LAK12	LAL12	3.40	7.2	13.0	23	9.7	Al7079TC

Table 2b. DEIMOS Camera: RTV560 width, thickness, shape factor, and α_e, and E_e for each camera lens.

Lens	Ohara Name	Width w (inches)	Thickness t (inches)	Shape S	R_{om} (inches)	α_e x 10^6 (/ ^{o}C)	E_e (psi)
1	LAL7	0.65	0.113	2.87	6.214	666	3158
4	BSM51Y	0.85	0.127	3.35	6.828	674	4107
6	PBL26Y	0.45	0.088	2.56	5.838	659	2610
7	BSM51Y	0.55	0.109	2.53	5.710	659	2572
8	FPL51	0.34	0.047	3.48	5.248	676	4372
9	LAL12	0.25	0.093	1.35	3.492	602	1108

We used Equations 7 and 8 to calculate stresses induced by design errors for each lens (Table 3). We assumed errors of 30%, 10%, and 3% in thermal expansion coefficients for RTV560, glass, and metal respectively. All thickness and stress values are for an assumed temperature change of 20 ^{o}C.

Table 3. Stresses induced by errors in thermal coefficients of expansion.

	$\delta a_e / a_e = 0.30$		$\delta a_g / a_g = 0.10$		$\delta a_m / a_m = 0.03$	
Lens	$M = \delta t_{eo}$ (mils)	σ (psi)	$M = \delta t_{eo}$ (mils)	σ (psi)	$M = \delta t_{eo}$ (mils)	σ (psi)
1	0.45	12.6	0.08	2.3	0.07	2.0
4	0.51	16.6	0.08	2.7	0.08	2.5
6	0.35	10.3	0.10	3.0	0.07	1.9
7	0.43	10.2	0.07	1.7	0.06	1.5
8	0.19	17.7	0.13	12.2	0.06	5.4
9	0.34	4.0	0.05	0.6	0.05	0.6

Optical Impact of the Error-Induced Stress

We have made finite-element calculations of the lens surface deformations resulting from the stresses in Table 3. Focus and spherical aberrations are induced in the surfaces. We have scaled those results to the quadrature sum of the pressures in Table 3. Table 4 gives the fractional change in power ($\delta F/F$) and the diameter of the spherical aberration blur circle (ASPH) if we assume each lens is standing alone and not in the camera. We have calculated deformations for only the most sensitive lenses, those with a meniscus shape.

Table 4. Fractional change in power and diameter of spherical aberration blur circle, assuming each lens stands alone, i.e. not in a camera.

Lens	$\delta F/F$ x 10^{+6}	ASPH (microns)
1	-2.17	2.1
4	-0.20	-0.6
6	-1.75	1.1
7	-0.47	-0.9

The rms design diameter of the DEIMOS images over the FOV is 23 microns. Thus, we conclude that the errors assumed in Table 3 will have a negligible impact on the optical performance.

7. RESPONSE TO LOADS: STATIC AND DYNAMIC

We calculate here the mass and moments of inertia of a lens and use these to calculate the resonant frequencies of the lens in an elastomer mount.

Define a lens by conic surfaces S1 and S2, central thickness "t", maximum radius "a", and density "d." Define a cylindrical coordinate system with the origin at the midpoint of the central thickness.

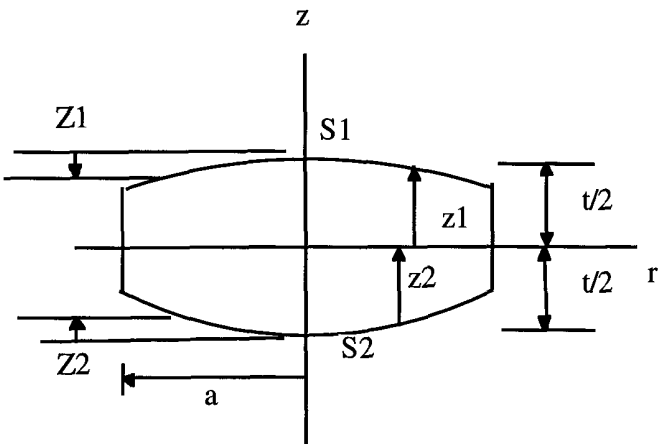

Figure 3

The arrows indicate the positive direction for the distances Z and z.

We can describe any conic surface (radius of curvature=k,conic constant = K) by a polar monomial series.

$$Z(r) = \sum_{n=1}^{\infty} a_{2n}\,\rho^{2n} \qquad \text{where } \rho \equiv \frac{r}{a} \qquad \text{and } Z(0) = 0 \qquad \text{and} \tag{14}$$

$$a_2 = \frac{a^2}{2k}\ ,\ a_4 = (K+1)\frac{a^4}{8k^3}\ ,\ a_6 = (K+1)^2\frac{a^6}{16k^5}\ ,\ a_8 = (K+1)^3\frac{5a^8}{128k^7}\ ,\ \ldots \tag{15}$$

$k < 0$ concave $\qquad k > 0$ convex

$K = 0 \Rightarrow$ sphere. $\qquad K = -1 \Rightarrow$ parabola.

The most steeply curved lens of DEIMOS is Element # 5, a sphere (K = 0) with a = 5.70 inches, k = 6.09 inches, and $(a/k)^2 = 0.88$. For calculations of mass and moments we typically need ~10% accuracy. For even this extreme case, we need to use only the first two terms in the series.

Define

$$z_1(\rho) \equiv +\frac{t}{2} - Z_1(\rho)\ , \qquad Z_1(\rho=0) = 0\ ,$$

$$z_2(\rho) \equiv -\frac{t}{2} + Z_2(\rho)\ , \qquad Z_2(\rho=0) = 0\ . \tag{16}$$

$$h(m) \equiv \int_0^1 Z(r)\,\rho^m\,d\rho\ ; \qquad f(k) \equiv \int_0^1 Z(r)^k\,\rho\,d\rho\ . \tag{17}$$

Assuming only two terms in Z (a_2 and a_4) yields

$h(0) = a_2/3 + a_4/5\ , \qquad f(0) = 1\ ,$

$h(1) = a_2/4 + a_4/6\ , \qquad f(1) = a_2/4 + a_4/6 = h(1)\ ,$

$h(2) = a_2/5 + a_4/7\ , \qquad f(2) = a_2^2/6 + a_2 a_4/4 + a_4^2/10\ ,$

$$h(3) = a_2/6 + a_4/8\ , \qquad f(3) = a_2^3/8 + 3a_2^2 a_4/10 + 3a_2 a_4^2/12 + a_4^3/14\ . \tag{18}$$

Integrating yields the following:

Mass

$$M = d\pi a^2\ [\,t - 2h_{S1}(1) - 2h_{S2}(1)\,] \tag{19}$$

Center of gravity (with respect to the origin) in the z direction

$$CG = d\pi a^2\ [\,t\,(h_{S2}(1) - h_{S1}(1)\,) + f_{S1}(2) - f_{S2}(2)\,]\,/\,M \tag{20}$$

Moment of inertia about z-axis

$$I_z = d\pi a^4\ [\,t - 2h_{S1}(3) - 2h_{S2}(3)\,] \tag{21}$$

Moment of inertia about x-axis (or y-axis)

$$I_x = d\frac{\pi}{6}a^2\{t^3 - 3t^2[f_{S1}(1)+f_{S2}(1)] + 6t[f_{S1}(2)+f_{S2}(2)] - 4\,[f_{S1}(3)+f_{S2}(3)]\} + \frac{1}{2}I_z \tag{22}$$

Displacements under gravity in the z and x directions

$$\Delta z = \frac{t\,Mg}{G_e 2\pi R_e w}\ , \qquad \Delta x = \frac{t\,Mg}{\pi w a (E_e + G_e)}\ , \tag{23}$$

where the t, w are the bond dimensions and E_e and G_e are evaluated for the shape factor of the bond.

We note that our expression for Δx differs from one often cited from Valente and Richard (1991). Their expression is an approximation for an assumed shape factor.

Resonant Frequencies Define $R_e \equiv (R_g + R_m)/2$

$$f_{axial} = \left(\frac{G_e R_e w}{2\pi t M}\right)^{1/2} \qquad f_{transverse} = \left(\frac{(E_e+G_e)R_e w}{\pi t M}\right)^{1/2}$$

$$f_{rotational} = \left(\frac{G_e R_e^3 w}{2\pi t I_z}\right)^{1/2} \qquad f_{tip/tilt} = \left(\frac{G_e R_e^3 w}{4\pi t I_x}\right)^{1/2} \tag{24}$$

Table 5 gives the masses, center of gravity, moments of inertia, and displacements under gravity of the DEIMOS lenses using Equations 14 to 23.

Table 5. Masses, Moments of Inertia, and Displacements in Gravity.

Lens	M (kg)	CG (mm)	I_z (kgm^2)	$I_x = I_y$ (kgm^2)	Δz (microns)	Δx (microns)
1	9.2	-12	0.14	0.073	1.0	1.1
4	10.5	-48	0.21	0.137	1.4	1.5
6	4.2	-17	0.07	0.039	0.7	0.7
7	5.7	-33	0.091	0.054	0.9	1.0
8	11.1	-7	0.24	0.139	0.8	0.9
9	1.3	+4	0.006	0.003	0.6	0.7

The small displacements Δz and Δx, ~ 1 micron, demonstrate the stiffness of the mounts. We note that the dispacements here are calculated assuming the lens is only constrained by the elastomer. In practice, the axial stiffness of provided by stops and preloads. The displacement Δz in Table 5 is calculated

assuming a full gravity load. The DEIMOS camera is only 3^{o} from horizontal; thus the axial gravity load seen by the lenses is 20 times smaller.

Table 6 gives the resonant frequencies for above designs using Equation 24.

Table 6. Resonant Frequencies

Lens	f_{axial} (Hz)	$f_{transverse}$ (Hz)	$f_{rotational}$ (Hz)	$f_{tip/tilt}$ (Hz)
1	337	952	426	591
4	286	809	170	213
6	414	1170	459	635
7	346	979	393	513
8	371	1048	342	448
9	417	1181	518	725

The resonant frequencies vary from about 200 to 1200 Hz. As expected from the displacements, these mounts are stiff.

A more detailed description of the material in this paper will be published in a UCO/Lick Observatories Technical Report.

8. REFERENCES

Epps, Harland W. "Adopted Preconstruction Optical Design for the DEIMOS 15.0-Inch f/1.29 Camera Lens, 30 March 1995 (private communication).

Faber, Sandra; Hilyard, David; James, Eric; Pfister, Terry "The design and assembly of camera lens cells for fluid couplants using elastomeric lens mounts", University of California UCO/Lick Observatory Technical Report No. 79 (August 1996).

Fata, Robert and Fabricant, Daniel "Design of a cell for the wide-field corrector for the converted MMT", Proceedings of the SPIE, Volume 1998, pp 32-38, 1993.

Gent, A.N. and Lindley, P. B. "The Compression of Bonded Rubber Blocks" Proc. Instn. Mech. Engrs., Volume 173, 3, 111 (1959).

Lindley, P. B. "Engineering Design With Natural Rubber" Natural Rubber Producer's Research Association (1972).

Lobdell, A. J. "Effect of Shear Restraint on the Properties of RTV-11, "Itek Interoffice Memorandum", November 13, 1968.

Valente, T.M. and R. M. Richard, 1991, "Analysis of elastomer lens mountings" Optomechanics and Dimensional Stablity, Proceedings of the SPIE, Volume 1533, Paquin, R. A. and Vukobratovich, D. (Eds.) p 21.

Yoder, Paul R. *Opto-Mechanical Systems Design*, Second Edition, Marcel Dekker, Inc. New York, 1993, and also Chapter 6 "Optical Mounts: Lenses, Windows, Small Mirrors, and Prisms" in *Handbook of Optomechanical Engineering*, editor Anees Ahmad, CRC Press, 1997.